Reversal of Neuropathic Pain in Diabetes by Targeting Glycosylation of $Ca_V3.2$ T-Type Calcium Channels

Peihan Orestes,[1,3] Hari Prasad Osuru,[1] William E. McIntire,[4] Megan O. Jacus,[1] Reza Salajegheh,[1] Miljen M. Jagodic,[1] WonJoo Choe,[1,6] JeongHan Lee,[1,7] Sang-Soo Lee,[8,9] Kirstin E. Rose,[1] Nathan Poiro,[1] Michael R. DiGruccio,[1,3] Katiresan Krishnan,[5] Douglas F. Covey,[5] Jung-Ha Lee,[8,9] Paula Q. Barrett,[4] Vesna Jevtovic-Todorovic,[1,2,3] and Slobodan M. Todorovic[1,2,3]

It has been established that $Ca_V3.2$ T-type voltage-gated calcium channels (T-channels) play a key role in the sensitized (hyperexcitable) state of nociceptive sensory neurons (nociceptors) in response to hyperglycemia associated with diabetes, which in turn can be a basis for painful symptoms of peripheral diabetic neuropathy (PDN). Unfortunately, current treatment for painful PDN has been limited by nonspecific systemic drugs with significant side effects or potential for abuse. We studied in vitro and in vivo mechanisms of plasticity of $Ca_V3.2$ T-channel in a leptin-deficient (*ob/ob*) mouse model of PDN. We demonstrate that posttranslational glycosylation of specific extracellular asparagine residues in $Ca_V3.2$ channels accelerates current kinetics, increases current density, and augments channel membrane expression. Importantly, deglycosylation treatment with neuraminidase inhibits native T-currents in nociceptors and in so doing completely and selectively reverses hyperalgesia in diabetic *ob/ob* mice without altering baseline pain responses in healthy mice. Our study describes a new mechanism for the regulation of $Ca_V3.2$ activity and suggests that modulating the glycosylation state of T-channels in nociceptors may provide a way to suppress peripheral sensitization. Understanding the details of this regulatory pathway could facilitate the development of novel specific therapies for the treatment of painful PDN. ***Diabetes*** **62:3828–3838, 2013**

Despite significant advances in glucose monitoring and insulin therapy, people with diabetes remain hyperglycemic during significant portions of the day, placing them at increased risk for the development of diabetes complications including peripheral diabetic neuropathy (PDN). One of the notable features of early PDN is the development of chronic neuropathic pain manifested as allodynia and hyperalgesia (1–3). Unfortunately, currently available therapies have limited efficacy or serious side effects. For example, gabapentin and pregabalin can relieve symptoms of painful PDN; however, >50% of patients using these drugs experience side effects, most notably excessive sedation, which limits their clinical use (2). Although opioids and nonsteroidal pain killers are also partially effective for treatment of chronic painful disorders, their long-term use is associated with side effects like gastrointestinal bleeding, tolerance, and addiction. Hence, further research to develop mechanism-specific novel pain therapies is warranted.

Recent studies have established the importance of the $Ca_V3.2$ subtype of T-channels in controlling the excitability of peripheral nociceptors in dorsal root ganglia (DRG) and supporting peripheral pain processing in animal models of PDN (4). Despite these interesting findings, no pharmacological approach targeting these channels has provided a significant therapeutic benefit to these patients. This is in part because the mechanisms underlying DRG T-channel plasticity in chronic pain disorders, like PDN, remain unknown. Here, we hypothesize that posttranslational modification of $Ca_V3.2$ channels in nociceptors via glycosylation contributes to painful symptoms in an animal model of PDN.

RESEARCH DESIGN AND METHODS

Ethics approval was obtained for all experimental protocols from the University of Virginia Animal Care and Use Committee, Charlottesville, Virginia. All experiments were conducted in accordance with the *Guide for the Care and Use of Laboratory Animals* adopted by the National Institutes of Health. Every effort was made to minimize animal suffering and the number of animals used. We used our standard procedure for testing mechanical and thermal sensitivity as we previously described (5). Statistical comparisons were made using one- and two-way repeated ANOVAs (paw and time postinjection) followed by Holm-Sidak multiple comparison with statistical significance accepted at $P < 0.05$. All drug injections were performed in a blinded manner. ECN [(3β,5α,17β)-17-hydroxyestrane-3-carbonitrile] was dissolved in 15% β-cyclodextrin ([2-hydroxypropyl]-β-cyclodextrin) (Cyc) solution (Sigma-Aldrich), and 750 μL i.p. solution containing ECN or vehicle alone was injected.

Electrophysiological studies. Patch-clamp recordings from acutely dissociated DRG neurons and human embryonic kidney (HEK)-293 cells were described in detail in our previous publication (6). The external solution for voltage-clamp experiments in HEK-293 cell experiments contained (in millimoles) 152 TEA-Cl, 2–10 $BaCl_2$, and 10 HEPES, adjusted to pH 7.4 with tetraethyl ammonium hydroxide (TEA-OH). For voltage-clamp experiments in DRG cells, we used 2 mmol/L Ca^{2+} in external solution instead of Ba^{2+}. The external solution for current-clamp experiments and recordings of voltage-gated sodium currents contained (in millimoles) 140 NaCl, 4 KCl, 2 $MgCl_2$, 2 $CaCl_2$, 10 glucose, and 10 HEPES, adjusted to pH 7.4. The internal solution for voltage-clamp experiments with DRG neurons contained (in millimoles) 135 TMA-OH, 40 HEPES, 10 EGTA, and 2 $MgCl_2$, adjusted to pH 7.2 with hydrogen fluoride (7). The internal solution for voltage-clamp experiments with HEK-293 cells contained (in millimoles) 110 Cs-$MeSO_4$ 14 creatine phosphate, 10 HEPES, 9 EGTA, 5 Mg-ATP, and 0.3 Tris-GTP, adjusted to pH 7.3 with CsOH. The internal solution for current-clamp experiments contained (in millimoles)

From the [1]Department of Anesthesiology, University of Virginia Health System, Charlottesville, Virginia; the [2]Department of Neuroscience, University of Virginia Health System, Charlottesville, Virginia; the [3]Neuroscience Graduate Program, University of Virginia Health System, Charlottesville, Virginia; the [4]Department of Pharmacology, University of Virginia Health System, Charlottesville, Virginia; the [5]Department of Developmental Biology, Washington University School of Medicine, St. Louis, Missouri; the [6]Department of Anesthesiology and Pain Medicine, InJe University, Ilsan Paik Hospital & College of Medicine, Goyang-City, South Korea; the [7]Department of Anesthesiology and Pain Medicine, Busan Paik Hospital, InJe University, College of Medicine, Busan, South Korea; the [8]Department of Life Science, Sogang University, Seoul, South Korea; and the [9]Interdisciplinary Program of Biotechnology, Sogang University, Seoul, South Korea.

Corresponding author: Slobodan M. Todorovic, st9d@virginia.edu.

Received 22 May 2013 and accepted 22 June 2013.

DOI: 10.2337/db13-0813

This article contains Supplementary Data online at http://diabetes.diabetesjournals.org/lookup/suppl/doi:10.2337/db13-0813/-/DC1.

See accompanying commentary, p. 3658.

130 KCl, 40 HEPES, 5 $MgCl_2$, 2 Mg-ATP, 1 EGTA, and 0.1 Na_3GTP, adjusted to pH 7.3 with KOH.

Statistical comparisons were made using paired or unpaired *t* tests where appropriate. All data are expressed as means ± SEM; *P* values are reported only when statistically significant (<0.05).

Biochemical studies

Construction of expression vectors. cDNA encoding the human Cav3.2 gene was subcloned into the mammalian expression vector pDoubleTrouble (8), resulting in hexahistidine and FLAG tags at the NH_2-terminal of the channel.

Cell culture and transfection. HEK-293 cells were cultured in Dulbecco's modified Eagle's medium containing 10% FBS. Stable cell lines expressing the epitope-tagged Cav3.2 channel were selected using the above media containing 500 μg/mL G418. Alternatively, the pDoubleTrouble vector containing Cav3.2 was used to transiently transfect cells. Fifteen-centimeter plates were transfected with 35 μg each of Cav3.2 DNA and Lipofectamine 2000 at a ratio of 1:1 and harvested at 48 h.

Deglycosylation in vitro. Purified $_{6HIS/FLAG}$Cav3.2 channel was separately incubated with PNGase F (New England Biolabs) and endoglycosidases (Endo) F1, F2, and F3 (Sigma) for 1 h at 37°C according to the manufacturers' instructions. Reactions were terminated by the addition of sample buffer.

Methods for purification of $Ca_V3.2$ channels and SDS-PAGE and immunoblotting are described in the Supplementary Data.

Immunostaining and imaging. Confocal images were acquired using a Zeiss 510UV confocal microscope and LSM ImageExaminer software. Single-plane images were taken using a 100× oil-immersion objective. For quantification of images, the colocalization plug-in for ImageJ (NIH) was used.

Construction of $Ca_v3.2$ N-glycosylation mutants. $Ca_v3.2$ N-glycosylation mutants (N192Q, N271Q, and N1466Q) were generated by mutating Asn^{192}, Asn^{271}, and Asn^{1466} residues of human $Ca_v3.2$ (GenBank accession no. AF051946) into Gln residues using two-step PCR methods. The specific methods are described in the Supplementary Data.

RESULTS

Recombinant $Ca_V3.2$ channels expressed heterologously in HEK-293 cells are typically cultured in a high-glucose medium to provide the cells' energy supply. Interestingly, we determined that the glucose level in Invitrogen's Dulbecco's modified Eagle's medium routinely used to grow these cells is 315 mg/dL (17.5 mmol/L) glucose—a value similar to blood glucose levels in diabetic *ob/ob* mice (5). We hypothesized that exposure of recombinant $Ca_V3.2$ channels to neuraminidase (NEU) (1.5 units/mL for 1–3 h at 37°C), an enzyme that deglycosylates proteins by removing sialic acid residues, would alter T-currents. We first characterized the effects of NEU on the current-voltage (I-V) relationship. We found that depolarization to different test potentials (V_t) from a holding potential (V_h) of −90 mV resulted in similar normalized I-V relationships in control (top traces, Fig. 1*A*) and NEU-treated (bottom traces, Fig. 1*A*) cells (untreated cells, $n = 18$; NEU-treated cells, $n = 13$ [Fig. 1*B* and *C*]). Nevertheless, we found a visible slowing of macroscopic current kinetics of activation (as measured by 10–90% rise time) and inactivation (as measured by inactivation τ) after treatment with NEU in comparison with control, untreated cells (Fig. 1*C* and *D*) with a dramatic twofold slowing of the τ of inactivation. We also examined the effects of PNGase-F (PNG) (20 units/cc for 12 h at 37°C), an enzyme that selectively cleaves N-glycosylated groups on proteins. Like NEU, PNG exposure slowed the kinetics of current activation and inactivation by twofold (gray columns, Fig. 1*E*). Additionally, we found that treatment with NEU or PNG also reduced peak current density by ~40% but that in combination, these agents were not more effective (Fig. 1*F*). Taken together, these data strongly suggest that NEU and PNG may share a common mechanism of modification of $Ca_V3.2$ channels.

Extracellular loops of ion channels may contain multiple potential motifs for glycosylation, which typically consist of an asparagine (Asn, N) residue separated from a serine (Ser, S) or threonine (Thr, T) residue by one amino acid (9). In $Ca_V3.2$ channels, conserved extracellular Asn residues in positions 192 (N192) and 271 (N271) of domain I and 1466 (N1466) of domain III are excellent candidate sites for N-glycosylation (Fig. 2*A*). We hypothesized that $Ca_V3.2$ channels with mutated critical Asn residues reared in high-glucose medium would have slower macroscopic kinetics of activation and inactivation than wild-type (WT) $Ca_V3.2$ channels. To test this hypothesis, we generated single-point mutants of $Ca_V3.2$ channels in which one Asn reside was mutated into a glutamine (Q), namely, N192Q, N1466Q, and N271Q. Using transiently transfected HEK-293 cells, we first compared the sensitivity of currents carried by N192Q mutant and WT $Ca_V3.2$ channels to nickel, a traditional $Ca_V3.2$ blocker. Traces depicted in Fig. 2*B* show that 100 μmol/L nickel applied in the external solution almost completely blocked inward currents carried by WT (top traces) and mutant (bottom traces) channels. Hence, N192Q mutation did not alter a signature pharmacological property of $Ca_V3.2$ channels. Nevertheless, consistent with a functional role for putative N192 glycosylation in channel activity, macroscopic current kinetics of activation and inactivation of N192Q mutant channels ($n = 15$) were significantly slower than those of WT channels ($n = 22$; $P < 0.001$) (Fig. 2*C*). Interestingly, current density (V_h −90 mV, V_t −30 mV) in N192Q channel mutant (17 ± 5 pA/pF, $n = 13$) was not different from WT $Ca_V3.2$ channel (15 ± 3 pA/pF, $n = 7$, $P > 0.05$). In contrast to the N192Q channel mutant, currents were not evident in recordings of N271Q and N1466Q channel mutants ($n \geq 10$, data not shown).

We next hypothesized that glycosylation state may regulate plasma membrane expression of $Ca_V3.2$ channels. To test this hypothesis, we constructed green fluorescent protein–tagged WT $Ca_V3.2$ channels (enhanced green fluorescent protein [EGFP]-$Ca_V3.2$) and mutant channels containing disrupted putative glycosylation motifs, (EGFP-N192Q, EGFP-N271Q, and EGFP-N1466Q), expressed them in HEK-293 cells, and used confocal microscopy to quantify immunofluorescence. Figure 3 illustrates a representative experiment from each channel type (WT $Ca_V3.2$ [Fig. 3*A*] and mutant channels [Fig. 3*B–D*]) showing red immunofluorescence for the structural membrane protein concanavalin A (*left panels*, Fig. 3*A–D*) and green immunofluorescence for the EGFP-tagged channel protein (*middle panels*, Fig. 3*A–D*). As indicated by the merging of red and green fluorescence (yellow color on *right panels* of Fig. 3*A–D*), we found that EGFP colocalized well with concanavalin A for WT (Fig. 3*A*) as well as N192Q (Fig. 3*B*) and N271Q (Fig. 3*C*) channel mutants consistent with predominant plasma membrane expression of these channel constructs. In contrast, the EGFP-N1466Q mutant channel was expressed predominantly in cytoplasmic organelles in agreement with lack of colocalization of the fluorescent signals (*right panel*, Fig. 3*D*). Average data from similar experiments were quantified blinded with arbitrary colocalization values and are summarized in Fig. 3*E*. Colocalization values were not significantly different for N192Q and N271Q mutants compared with WT $Ca_V3.2$ channels. By contrast, there is a large decrement in colocalization for N1466Q mutant: 28% of that of WT $Ca_V3.2$ channels ($n = 4$, $P < 0.01$), corroborating the lack of T-currents measured in our patch-clamp experiments in HEK cells expressing the N1466Q mutant.

Since two of our point mutations are located in repeat I of $Ca_V3.2$ channels (Fig. 2*A*), we generated NH_2-terminal FLAG-tagged$Ca_V3.2$ channels ($_{6HIS/FLAG}Ca_V3.2$) to enable ensuing biochemical studies. We used the FLAG tag to

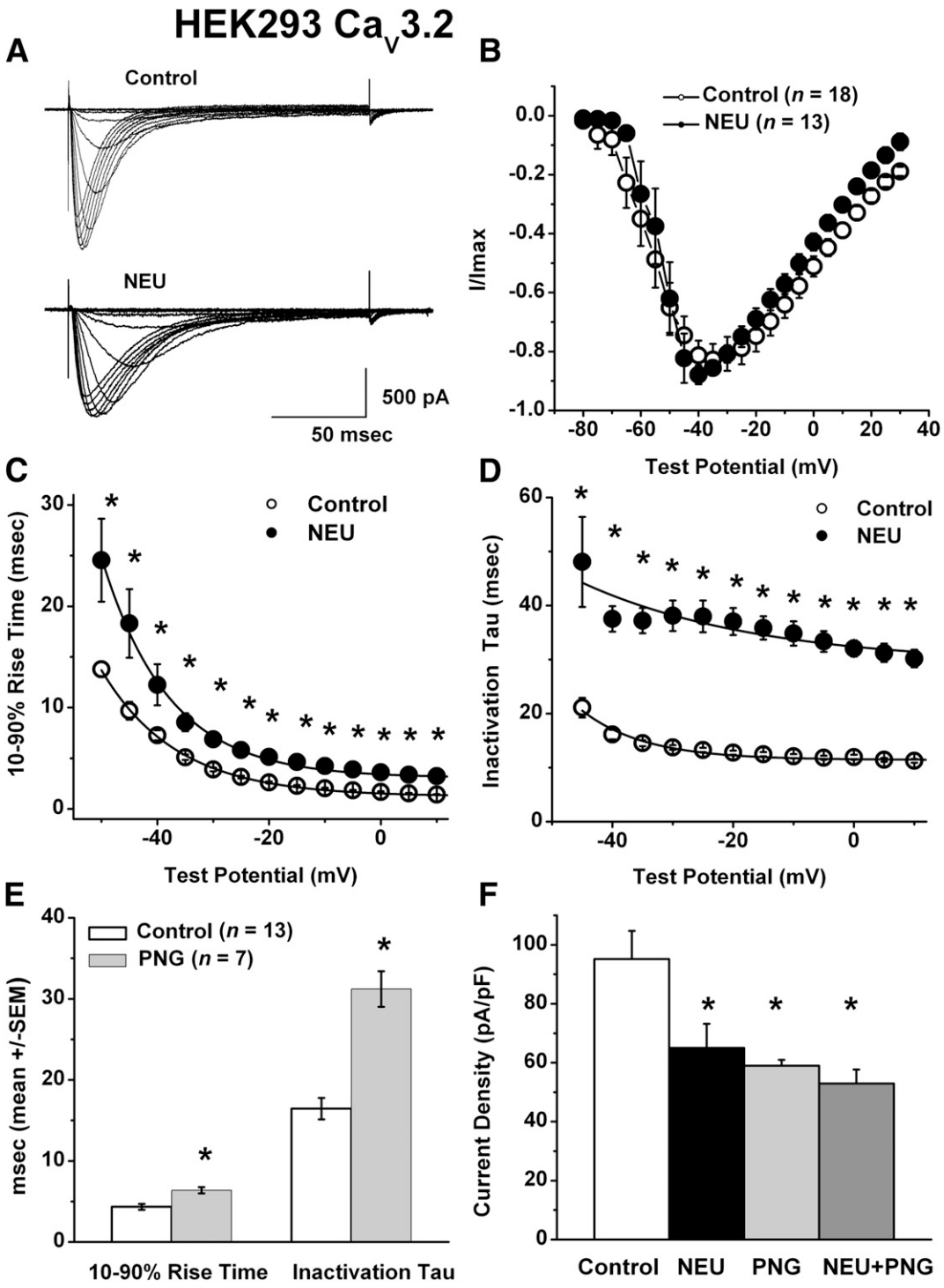

FIG. 1. NEU and PNG modulate recombinant human $Ca_V3.2$ channels. *A*: Traces represent families of T-currents evoked in representative HEK-293 cells in control conditions (*top panel*) and after incubation of 1.5 units/mL NEU at 37°C for 3 h (*lower panel*) by voltage steps from –90 mV (V_h) to V_t from −80 through −20 mV in 5-mV increments. Bars indicate calibration. *B*: Average normalized I-V curves (current/maximum current, I/Imax) are shown in HEK-293 cells in control conditions (n = 18) and after incubations of NEU (n = 13). *C* and *D*: We measured time-dependent activation (10–90% rise time [*C*]) and inactivation τ (single exponential fit of decaying portion of the current waveforms [*D*]) from I-V curves in HEK-293 cells (*B*) over the range of test potentials from −50 mV to 10 mV. There are differences in up to twofold slower times between the control and NEU groups at each tested potential. *Significance of $P < 0.05$. *E*: Bars represent 10–90% current activation rise times and current inactivation τ (V_h = −90 mV, V_t = −30 mV) measured in control cells (n = 13) and cells incubated with PNG (20 units/mL at 37°C for 12 h) (n = 7). Note that PNG-treated cells had slower activation and inactivation kinetics. *Significance of $P < 0.01$. *F*: Bar graphs depict peak current density (V_h = −90 mV, V_t = −30 mV) measured in multiple HEK-293 cells in control conditions (n = 20) and cells after incubation of NEU alone (n = 18), PNG alone (n = 7), and combined PNG and NEU (n = 11). Note that all three treatments significantly decreased peak current density compared with control cells: control 95 ± 10 (open bar, n = 20), NEU 65 ± 8 (n = 18, $P < 0.01$), PNG 59 ± 2 (n = 7, $P < 0.01$), and NEU plus PNG 53 ± 5 (n = 11, $P < 0.01$). *Significance of $P < 0.05$. Vertical bars in all panels represent SEM from multiple determinations.

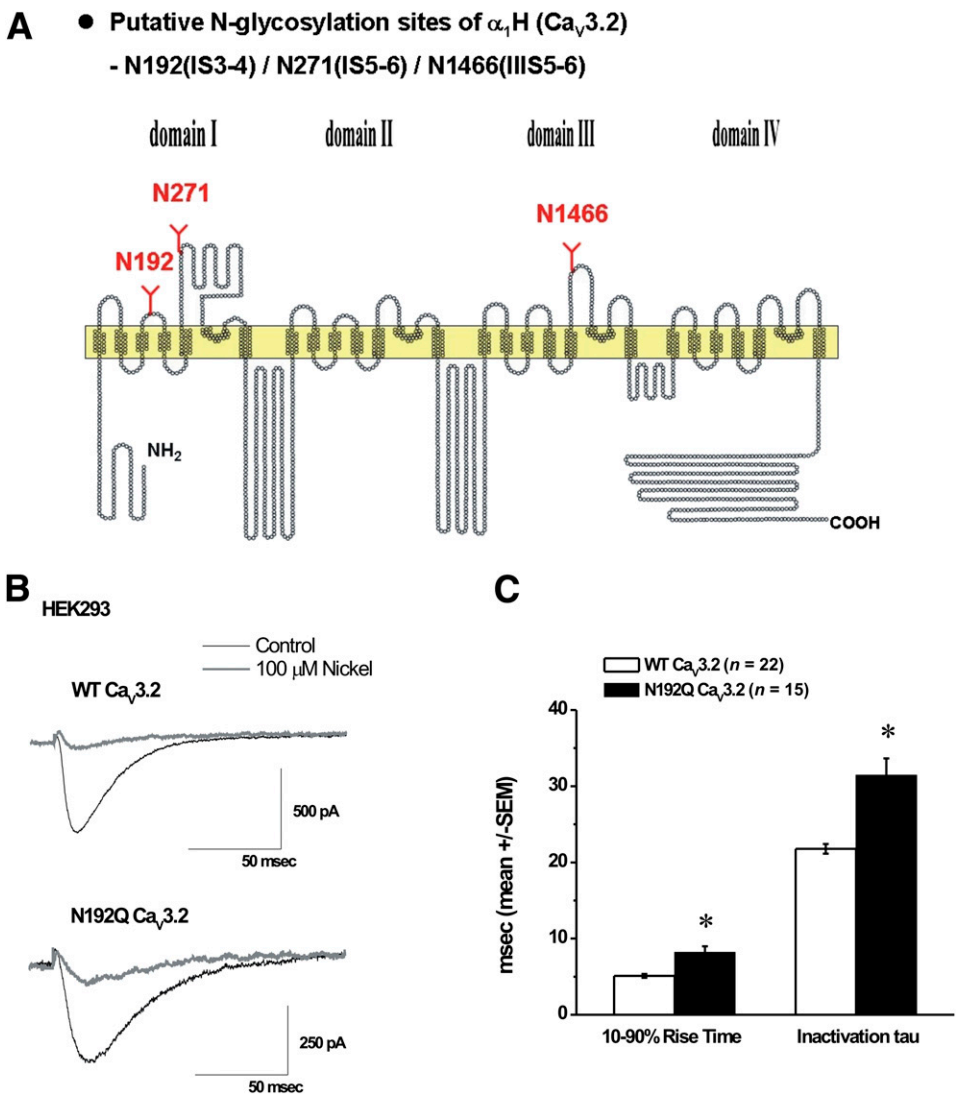

FIG. 2. Molecular mechanisms of glycosylation of Ca_V3.2 channels. *A*: Schematic diagram of Ca_v3.2 showing the position of conserved putative N-glycosylation sites in the extracellular face of the channel in domains I and III. Designated asparagine residues (in red bold fonts) were mutated to alanine residues. *B*: Representative traces in gray show nickel inhibition of T-current (black traces) in HEK-293 cell transiently transfected with WT Ca_V3.2 (*top*) and N192Q Ca_V3.2 (*bottom*) channels. In both experiments, 100 μmol/L $NiCl_2$ was applied in the bath. On average, nickel blocked 97 ± 2% of inward currents of N192Q Ca_V3.2 (n = 5) and WT Ca_V3.2 (n = 6) channels. Bars indicate calibration. *C*: Bar graph represents the average effect of N192Q Ca_V3.2 mutation compared with WT Ca_V3.2 T-current kinetics (V_h = −90 mV, V_t = −30 mV) in HEK-293 cells. On average, N192Q mutant has slower 10–90% rise times by ~60% (8.2 ± 0.8 s) compared with WT Ca_V3.2 currents (5.1 ± 0.2 s). Similarly, on average N192Q mutant has slower inactivation τ-values by ~50% (31.4 ± 2.2 s) compared with WT Ca_V3.2 currents (21.8 ± 0.6 s). Vertical lines are ±SEM of multiple determinations. Number of cells in each experiment is indicated in parentheses. *Significance of P < 0.001.

immunoprecipitate the $_{6HIS/FLAG}Ca_V3.2$ channel from HEK-293 cells grown in high glucose. Next, we treated the purified $_{6HIS/FLAG}Ca_V3.2$ channel with enzymes such as PNG and Endo F1, F2, and F3. Deglycosylation of proteins can result in a faster electrophoretic mobility and, thus, a lower apparent molecular weight. In the case of the full-length Ca_V3.2 channel (~260 kDa), very little change in electrophoretic mobility was observed after treatment with these enzymes (top arrow, Fig. 4), likely due to the large size of the protein. However, a small NH_2-terminal fragment of the Ca_V3.2 channel recognized by the FLAG antibody shifted its electrophoretic mobility after treatment with PNG and Endo F1 consistent with a change in apparent molecular weight from 60 kDa to 50 kDa (bottom arrow, Fig. 4). In contrast, treatments of $_{6HIS/FLAG}Ca_V3.2$ channel purified from HEK-293 cells with enzymes that are known to cleave complex carbohydrate molecules, such as Endo F2 and Endo F3, did not affect electrophoretic mobility of the NH_2-terminal fragment of Ca_V3.2 (bottom arrow, Fig. 4). Thus, our data strongly suggest that the Ca_V3.2 channel is glycosylated with a relatively simple sugar moiety within the first ~500 residues (50 kDa).

Next, we asked whether glycosylation may modulate native Ca_V3.2 currents in DRG nociceptors and may participate in painful PDN. Based on our recent studies using *ob/ob* mice, the upregulation of T-currents in small DRG neurons coincided with significant hyperglycemia, morbid obesity, and the development of painful PDN in mice aged 10–16 weeks (5). Thus, we first compared the biophysical properties of T-currents in acutely dissociated small DRG cells from diabetic *ob/ob* and healthy WT mice at age 10–16 weeks. Representative traces of T-currents in DRG cells from control (Fig. 5*A*) and *ob/ob* mice (Fig. 5*B*) indicate marked enhancement of their amplitudes in *ob/ob* mice

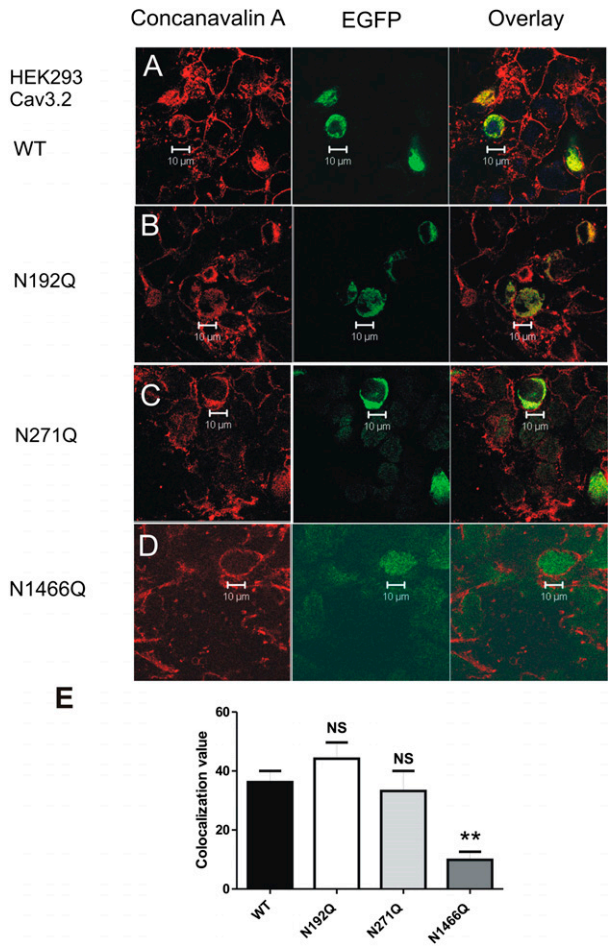

FIG. 3. Altered membrane expression of putative glycosylation sites in $Ca_V3.2$ channels. *A*: Representative confocal images in the *left panel* show HEK-293 cells transiently transfected with WT $Ca_V3.2$ channels where concanavalin A immunofluorescence is represented in red color. *Middle panel* shows green immunofluorescence representing EGFP-tagged $Ca_V3.2$ transfection in the same cells. *Right panel* shows merged images where overlay is presented in yellow color. *B*: Representative confocal images in the *left panel* show HEK-293 cells transiently transfected with N192Q $Ca_V3.2$ channels where concanavalin A immunofluorescence is represented in red color. *Middle panel* shows green immunofluorescence representing EGFP-tagged N192Q $Ca_V3.2$ transfection in the same cells. *Right panel* shows merged images where overlay is presented in yellow color. *C*: Representative confocal images in the *left panel* show HEK-293 cells transiently transfected with N271Q $Ca_V3.2$ channels where concanavalin A immunofluorescence was represented in red color. *Middle panel* shows green immunofluorescence representing EGFP-tagged N271Q $Ca_V3.2$ transfection in the same cells. *Right panel* shows merged images where overlay is presented in yellow color. *D*: Representative confocal images in the *left panel* show HEK-293 cells transiently transfected with N1466Q $Ca_V3.2$ channels where concanavalin A immunofluorescence was represented in red color. *Middle panel* shows green immunofluorescence representing EGFP-tagged N1466Q $Ca_V3.2$ transfection in the same cells. *Right panel* shows merged images where overlay is presented in yellow color. Note that EGFP and concanavalin A show very little overlap in their subcellular distributions. *E*: Bar graphs represent average values from multiple experiments (those depicted in *A–D*). Colocalization values for EGFP and concanavalin epifluorescence were quantified and compared between mutants and WT $Ca_V3.2$ channels. Only N1466Q mutants (dark-gray column, 9.9 ± 3.7, n = 4) displayed ~73% decrease in colocalization value compared with WT channels (black column, 36.2 ± 3.8, n = 4). In contrast, colocalization values of N192Q (open column, n = 4) and N271Q mutants (light gray bar, n = 3) were not significantly different from WT $Ca_V3.2$. **Statistically significant difference from $Ca_V3.2$ WT channels ($P < 0.01$). NS (not significant), $P > 0.05$ compared with $Ca_V3.2$ WT channels. Calibration bars are marked on all panels.

over the wide range of membrane potentials. We also found significant (up to twofold) speeding of the kinetics of macroscopic current inactivation and activation in *ob/ob* mice (n = 20 cells) compared with the WT group (n = 27 cells) at all potentials tested ($n \geq 6$ mice) (Fig. 5*C* and *D*). In contrast, there was no apparent difference between the two groups in the voltage dependence of activation (Fig. 5*E*) or inactivation (Fig. 5*F*) of T-currents. Shown in Fig. 6 are representative T-currents in DRG cells treated with NEU isolated from WT (top traces, Fig. 6*A*) or *ob/ob* (bottom traces, Fig. 6*A*) mice. Bar graphs in Fig. 6 summarize average data from similar experiments. Interestingly, treatment with NEU (filled columns) did not significantly change T-current density in cells from WT mice but effectively decreased T-current density in the *ob/ob* group to WT levels (~17 pA/pF) (Fig. 6*B*). Furthermore, NEU significantly slowed both WT and *ob/ob* control T-current kinetics to similar levels: τ of inactivation to ~105 ms and 10–90% rise time of ~28 ms (Fig. 6*C* and *D*).

We also tested the possibility that NEU may affect other parameters besides T-currents in *ob/ob* mice using voltage- and current-clamp recordings from small DRG cells of diabetic *ob/ob* mice. In these experiments, we blindly assigned saline-treated and NEU-treated dishes from the same preparations of DRG cells. Cells were first voltage clamped, and inward currents were evoked with a series of depolarizing pulses of 200 ms duration (V_h = −90 mV, V_t = −60 mV through 0 mV). We found no significant difference in the peak amplitude of voltage-gated sodium currents in two groups: saline 230 ± 28 pA/pF (n = 25 cells) and NEU 307 ± 46 pA/pF (n = 18 cells, $P > 0.05$, $n \geq 6$ mice per group). In ensuing current-clamp experiments in some of these cells, we injected a series of incremental hyperpolarizing pulses and we measured passive membrane properties such as soma diameter, membrane capacitance, input resistance, and resting membrane potential. Supplementary Table 1 summarizes these data and indicates that NEU treatment did not have significant effects on any of these parameters ($P > 0.05$).

We previously demonstrated that selective T-channel blocker ECN (10) at the dose of 25 mg/kg i.p. effectively reversed hyperalgesia in diabetic *ob/ob* mice and diabetic WT mice but had no effect on nociception in diabetic $Ca_V3.2$ knockout (KO) mice (5). However, the effects of NEU on pain thresholds in whole animals are not known. Hence, we examined whether NEU modifies in vivo sensitivity to mechanical and noxious thermal (heat) stimuli. We first measured baseline paw withdrawal responses (PWRs) in the presence of a mechanical stimulus elicited by von Frey filament (time point 0) and then injected (arrows, Fig. 7) 10 µL NEU or vehicle in the hind paws of WT (n = 5) or diabetic *ob/ob* (n = 10) mice. We then measured PWRs in both paws at 30, 60, and 90 min after injection. As confirmed in Fig. 7*A* and *B*, *ob/ob* mice had increased baseline paw withdrawal latencies (PWLs) of ~60% compared with their age-matched WT counterparts (Fig. 7*C* and *D*), suggestive of prominent mechanical hyperalgesia (5,11). Importantly, intraplantar (i.pl.) injection of 1.5 units/mL of NEU, the same concentration used in our in vitro experiments, completely reversed mechanical hyperalgesia in the injected (right) paws of *ob/ob* mice (Fig. 7*A*). In contrast, saline injections did not cause any significant changes in PWRs (Fig. 7*A*). Interestingly, there was a transient hyperalgesic response to injections of NEU in WT mice, while saline injections did not cause any alterations in baseline PWRs (Fig. 7*C*). PWLs in uninjected

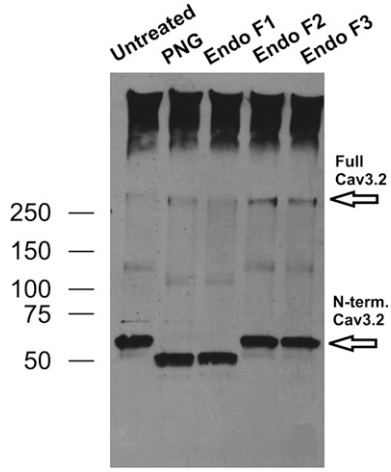

FIG. 4. Biochemical evidence of glycosylation of $Ca_V3.2$ channels. Immunoblotting with FLAG antibody reveals a shift in apparent molecular weight of NH_2-terminal fragment of $Ca_V3.2$ channel (bottom arrow) but not full channel (top arrow). Note that treatment with PNGase-F and Endo F1 but not Endo F2 and Endo F3 caused an obvious change in mobility of FLAG-labeled NH_2-terminal fragment of $Ca_V3.2$ from ~60 to 50 KDa. Using mass spectrometry, we confirmed that the deglycosylated NH_2-terminal fragment of $Ca_V3.2$ channels recognized by FLAG antibodies contains most of the repeat I of $Ca_V3.2$ channel (data not shown). N-term., NH_2-terminal.

(left) paws of *ob/ob* mice (Fig. 7*B*) and WT mice (Fig. 7*D*) remained stable throughout testing, indicating a lack of systemic effect. To test whether the antihyperalgesic effect of NEU in *ob/ob* mice is related to its effects on T-currents, we injected 25 mg/kg i.p. ECN ~60 min before i.pl. injections of NEU ($n = 8$) (Fig. 7*E*). As expected, the injections of ECN completely reversed mechanical hyperalgesia in *ob/ob* mice, as evidenced by a notable decrease of mechanical PWRs in both paws measured 60 min after injections ($P < 0.001$). Importantly, subsequent i.pl. injections of NEU did not further decrease PWRs in right paws. Unlike with ECN, the i.p. injections of Cyc (vehicle) did not change baseline mechanical PWRs in *ob/ob* mice and subsequent local injections of NEU into right paws significantly decreased PWRs up to ~50% (Fig. 7*F*). PWLs in uninjected (left) paws of the same *ob/ob* mice remained stable throughout testing, indicating a lack of systemic effect of NEU (Fig. 7*F*).

Next, we measured baseline PWL in the presence of a radiant heat stimulus (time point 0) and then injected (arrows, Fig. 8) 10 μL NEU or vehicle i.pl. in 16-week-old WT ($n = 7$) or *ob/ob* ($n = 7$) mice. *ob/ob* mice (*top panel*, Fig. 8*A*) had decreased baseline PWLs (4.0 ± 0.2 s) for ~20% compared with their age-matched WT counterparts (5.1 ± 0.3 s, $P < 0.01$) (*bottom panel*, Fig. 8*A*), indicating mild heat hyperalgesia (5). Importantly, injection of 1.5 units/mL NEU i.pl. produced a significant antihyperalgesia, as evident by an increase in PWLs only in *ob/ob* mice at 30 min after injection (*top panel*, Fig. 8*A*) but not in WT mice (*bottom panel*, Fig. 8*A*). In control experiments, the same volume of saline (vehicle) had no effect on thermal PWLs in either WT or *ob/ob* mice ($n \geq 7$, data not shown). As depicted in Fig. 8*B*, the intraperitoneal injections of ECN had analgesic effects in *ob/ob* mice as evidenced by a notable increase of thermal PWLs in both paws ($n = 4, P < 0.001$). Importantly, subsequent i.pl. injections of NEU did not further prolong PWLs in right paws.

DISCUSSION

It has been established that T-channels can contribute to the hyperexcitability of sensory neurons manifested by hyperalgesia and allodynia, two frequent symptoms of chronic neuropathic pain (4,12). Several studies have validated that plasticity of T-channels is implicated in hyperalgesia and allodynia in animal models of PDN (5,12–17). Taken together, these studies identify an important pronociceptive role of $Ca_V3.2$ T-channels in neuropathic pain in animal models of type 1 and type 2 diabetes.

However, molecular mechanisms for the alteration of $Ca_V3.2$ channels in DRG cells from diabetic animals have not previously been described. Indeed, herein, we provide evidence for the first time that targeting glycosylation states of T-channels may be a promising new treatment for painful PDN. This conclusion is based on several observations from our study. First, we show that macroscopic current activation and inactivation kinetics as well as current density are drastically reduced when recombinant human $Ca_V3.2$ channels expressed in HEK-293 cells reared in hyperglycemic cell culture medium are exposed to NEU and PNG. Second, the effects of NEU are more prominent in DRG cells from diabetic *ob/ob* mice than in healthy WT mice. Third, NEU in vivo completely reversed thermal and mechanical hyperalgesia in diabetic *ob/ob* mice, whereas it was completely ineffective in age-matched healthy WT mice. The fact that NEU modified DRG T-current kinetics from healthy WT mice but to a lesser extent than in *ob/ob* mice suggests that the level of T-channel glycosylation is an important physiological mechanism that fine-tunes the activity of these channels in pain pathways. However, it appears that this process is maladaptive and leads to cellular hyperexcitability and, consequently, hyperalgesia in diseases like PDN. Hence, glycosylation of $Ca_V3.2$ channels is an important mechanism of sensitization of peripheral nociceptors that could be exploited for novel pain therapies.

Our molecular studies identify conserved extracellular asparagine residues, most notably N192 and N1466, as important regulators of $Ca_V3.2$ current kinetics and channel membrane expression, respectively. This is supported by our patch-clamp recordings that demonstrated slower current kinetics in N192Q $Ca_V3.2$ mutant with apparently normal membrane expression. In contrast, we could not consistently record T-currents in HEK-293 cells transfected with N1466Q $Ca_V3.2$ mutant, and our imaging studies with the EGFP-tagged mutant showed minimal membrane expression. Thus, different glycosylation sites in $Ca_V3.2$ channels may have distinct functional roles. Surprisingly, we could not record T-currents from N271Q Cav3.2 channels despite apparently normal membrane expression. It remains possible that N271Q channels trafficked to the membrane are nonfunctional. During the review of our study, another in vitro study using recombinant human $Ca_V3.2$ channels also examined the effect of glycosylation on T-current kinetics and surface membrane expression (18). Surprisingly, they found that treatments with PNG but not NEU decreased $Ca_V3.2$ current density and slowed kinetics of channel inactivation. Furthermore, their work suggests that asparagine N192 serves as a regulator of channel membrane expression and asparagine N1466 as a regulator of channel kinetics. It is possible that specific conditions of enzymatic deglycosylation or different levels of glucose in cell culture could have contributed to the different findings between the studies. However, regardless of observed differences, our study directly demonstrates that

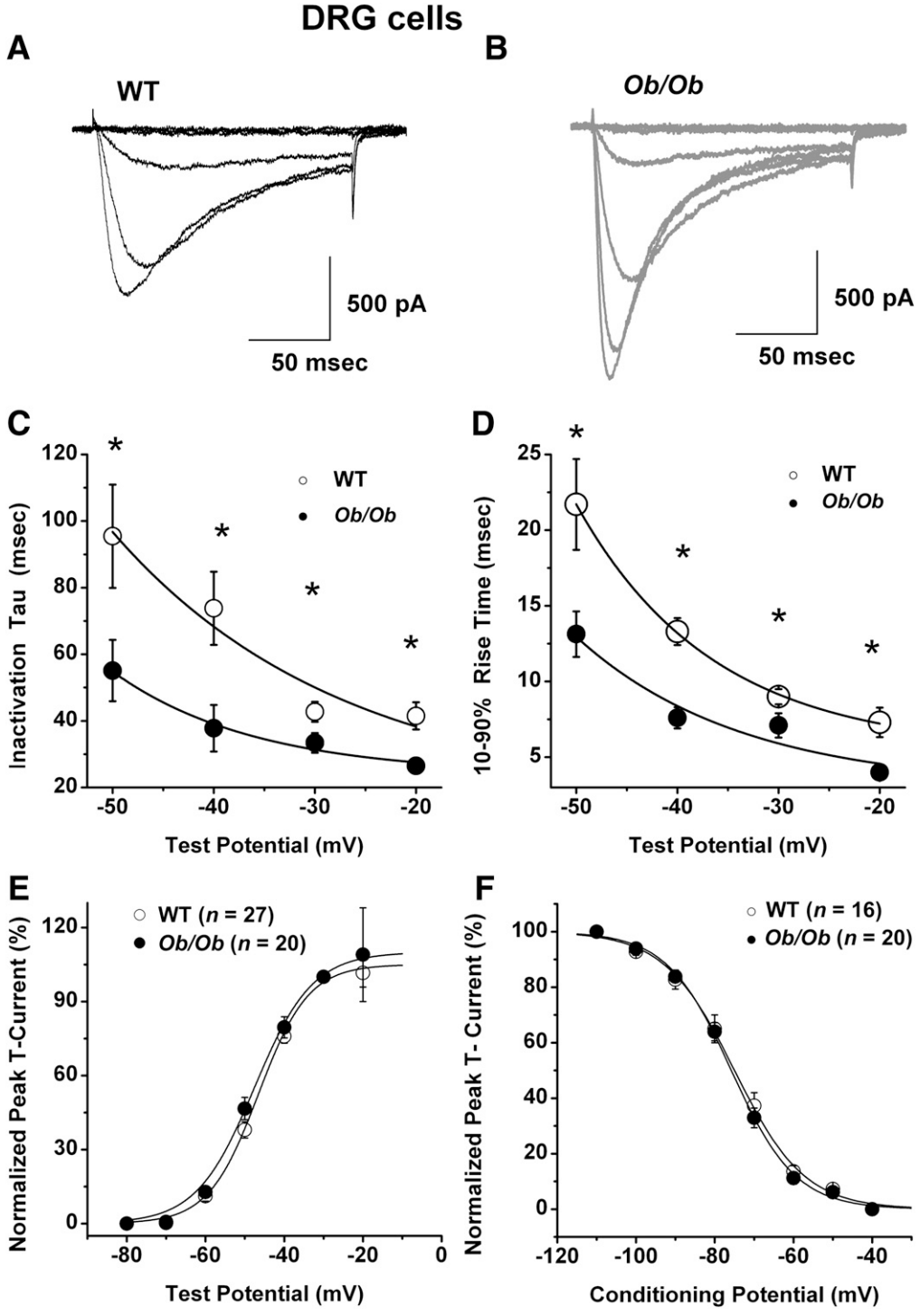

FIG. 5. Alterations of macroscopic T-current kinetics in acutely dissociated small DRG cells from diabetic *ob/ob* mice. The data show original T-current traces (V_h −90 mV, V_t −80 mV through −30 mV) from representative DRG cells from a healthy WT mouse (*A*) and a diabetic *ob/ob* mouse (*B*). The averaged data show marked acceleration in T-current inactivation (*C*) and activation (*D*) kinetics in *ob/ob* mice compared with age-matched WT mice. Data are averages of multiple cells (WT $n = 27$, *ob/ob* $n = 20$) ±SEM. *$P < 0.05$. Solid lines on *C* and *D* are single exponential fits to experimental data points. *E*: Normalized peak T-current activation curves from similar experiments shown in *A* and *B*. Number of cells is indicated in the parentheses. Solid black lines are fitted using equation 1, giving half-maximal activation (V_{50}), which occurred at −46.6 ± 0.6 mV with a k of 6.3 ± 0.5 mV in WT mice. Similarly, V_{50} was –47.6 ± 0.7 mV with a k of 7.4 ± 0.6 mV in the DRG cells from *ob/ob* mice. *F*: Normalized peak T-current steady-state inactivation curves. T-currents are evoked by test steps to −30 mV after 3.5-s prepulses to potentials ranging from −110 mV to −45 mV in 5-mV increments. Number of cells is indicated in the parentheses. Solid black lines are fitted using equation 2, giving V_{50}, which occurred at −75.0 ± 0.4 mV with a k of 8.9 ± 0.4 mV in WT mice. Similarly V_{50} was –75.8 ± 0.4 mV with a k of 8.2 ± 0.3 mV in the DRG cells from *ob/ob* mice. The voltage dependencies of activation and steady-state inactivation were described with single Boltzmann distributions of the following forms where I_{max} is the maximal activatable current, V_{50} is the voltage where half the current is activated or inactivated, and k is the voltage dependence (slope) of the distribution. Activation: $I(V) = I_{max}/\{1 + \exp[-(V - V_{50})/k]\}$ (1) Inactivation: $I(V) = I_{max}/\{1 + \exp[(V - V_{50})/k]\}$ (2), where exp = e^x.

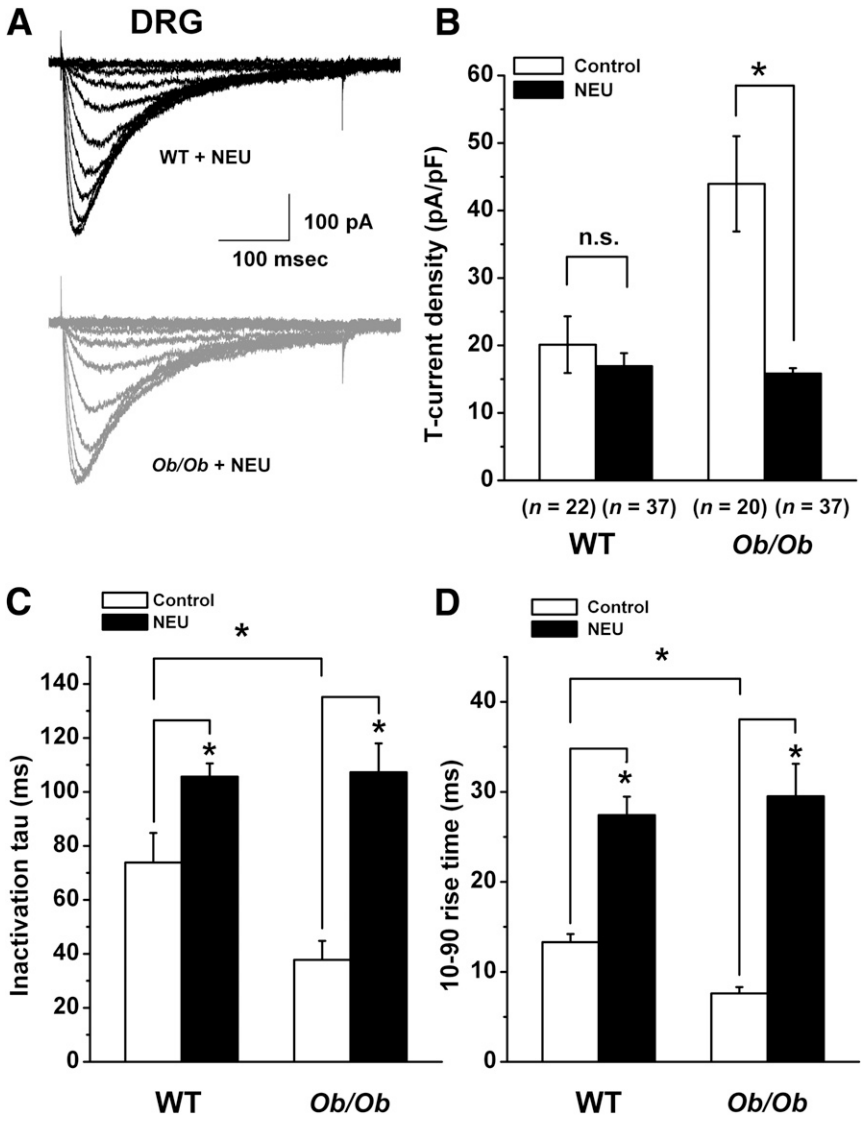

FIG. 6. NEU treatment in vitro reversed kinetic alterations and normalized T-current density in small DRG cells from diabetic *ob/ob* mice. *A*: Traces represent families of T-currents evoked in representative DRG cells in a WT mouse (*top panel*) and a diabetic *ob/ob* mouse after incubation of 1.5 units/mL of NEU at 37°C for 3 h (*lower panel*) by voltage steps from $V_h = -90$ mV to V_t from −80 through −25 mV in 5-mV increments. Bars indicate calibration. Bar graphs with the averaged data show that NEU treatments completely reversed DRG T-current density ($V_h = -90$ mV, $V_t = -30$ mV) (*B*), T-current inactivation measured by inactivation τ (*C*), and activation kinetics measured by 10–90% rise time (*D*) in *ob/ob* mice compared with healthy WT mice. Control was compared with post-NEU treatments. DRG cells were freshly dissociated as noted in Fig. 5. Recordings were performed at room temperature while NEU was incubated for 1–3 h at 37°C. Control cells were treated with saline. Data are averages of multiple cells (as indicated in parenthesis) ±SEM. *$P < 0.001$; n.s., not significant, $P > 0.05$.

$Ca_V3.2$ -channels are indeed glycosylated within domain I of the channel protein and for the first time reveals the prominent effects of NEU on native T-currents in DRG cells and on pain perception in vivo using an animal model of PDN.

Several other in vitro studies have reported that glycosylation may modulate properties of other voltage-gated ion channels. For example, in embryonic DRG neurons, NEU affected steady-state inactivation of voltage-gated sodium channels (19). While future biophysical studies may reveal fine details of the effects of glycosylation upon $Ca_V3.2$ current kinetics, it is reasonable to propose that increased current density and increased kinetics of $Ca_V3.2$ current activation alone may contribute to the hyperexcitable state of DRG cells under hyperglycemic conditions. Similar to the results of our study, the findings of Tyrrell et al. (19) did not show any effects of NEU on voltage-gated sodium channels in small DRG cells from adult animals. Future extensive electrophysiological studies could be expanded to involve examination of other voltage-gated channels that are crucial for the control of cellular excitability of DRG cells from diabetic animals that might also be modulated by glycosylation (20–22).

Previous in situ hybridization studies (23) and electrophysiological studies using KO mice (6,24) have established that the $Ca_V3.2$ is the most prevalent isoform of the Cav3.0 family in small DRG cells. Thus, we have focused our investigation on the effects of glycosylation on this particular isoform and on the peripheral sensitization of pain responses in PDN. Our molecular studies have found that extracellular asparagine residues N192 and N1466 are likely putative substrates for glycosylation that alter T-channel membrane expression and current kinetics. Since these asparagine residues are conserved across all

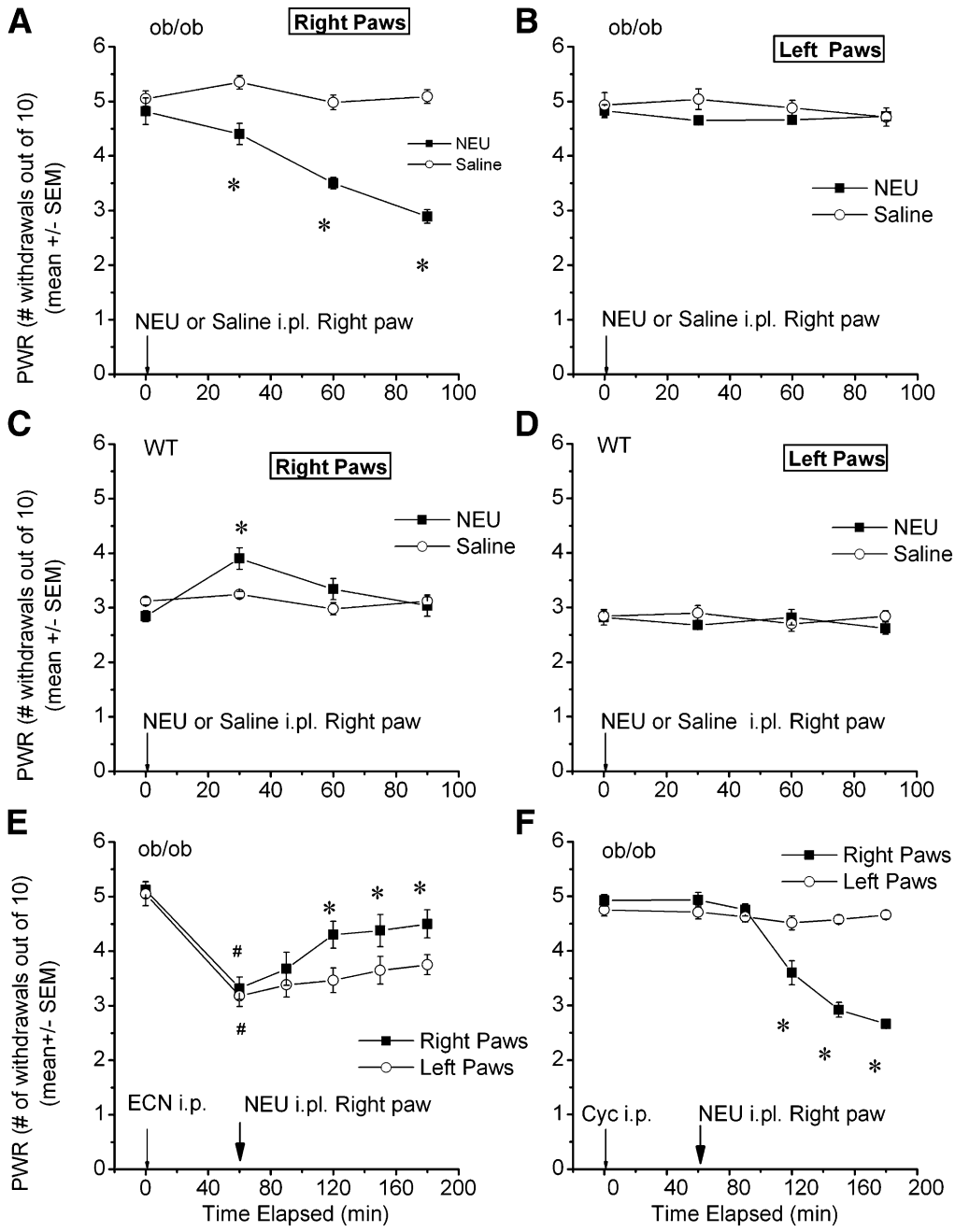

FIG. 7. NEU treatment in vivo reversed mechanical hyperalgesia in diabetic *ob/ob* mice. *A*: The graph shows average data points indicating that i.pl. injections of NEU but not saline into right paws completely reversed mechanical hyperalgesia in diabetic *ob/ob* mice. Arrow indicates time point of i.pl. injections. *Significant change of PWRs with $P < 0.05$ compared with baseline PWR prior to i.pl. injections. *B*: The graph shows average data points indicating that i.pl. injections of NEU and saline into right paws did not affect PWRs in the left paws of diabetic *ob/ob* mice. Arrow indicates time point of i.pl. injections. *C*: The graph shows average data points indicating that i.pl. injections of NEU but not saline into right paws caused transient hyperalgesia in healthy WT mice at the time point of 30 min. Arrow indicates time point of i.pl. injections. *Significant change of PWRs with $P < 0.001$ compared with baseline PWR prior to i.pl. injections. *D*: The graph shows average data points indicating that i.pl. injections of NEU and saline into right paws did not affect PWRs in the left paws of WT mice. Arrow indicates time point of i.pl. injections. *E*: The graph with averaged data from eight experiments shows that intraperitoneal injections (thin arrow) of selective T-channel blocker ECN (25 mg/kg i.p.) completely reversed mechanical hyperalgesia in diabetic *ob/ob* mice as evidenced by decreased PWRs in both right and left paws (#$P < 0.001$). Subsequent i.pl. injections (thick arrow) of 1.5 units/mL NEU in the same animals did not significantly influence new baseline values of mechanical PWRs at a time point of 90 min, but it significantly increased PWRs at time points of 120, 150, and 180 min (*$P < 0.05$). *F*: The graph with averaged data from eight experiments shows that intraperitoneal injections (thin arrow) of vehicle used to dissolve ECN (Cyc) did not affect mechanical hyperalgesia in diabetic *ob/ob* mice as evidenced by stable PWRs in both right and left paws at a time point of 60 min. Subsequent i.pl. injections (thick arrow) of 1.5 units/mL NEU in the same animals effectively reversed diabetic hyperalgesia by significantly decreasing PWRs at time points of 120, 150, and 180 min (*$P < 0.001$).

T-channel isoforms, it is likely that glycosylation may similarly modulate the other two T-channel isoforms, namely, $Ca_V3.1$ and $Ca_V3.3$. Interestingly, all three isoforms of T-type channels are expressed in dorsal horn neurons of spinal cord (23), and recent studies have shown that they all may support spinal nociceptive processing in different animal models of neuropathic pain (12,25,26). Thus, simultaneous glycosylation of

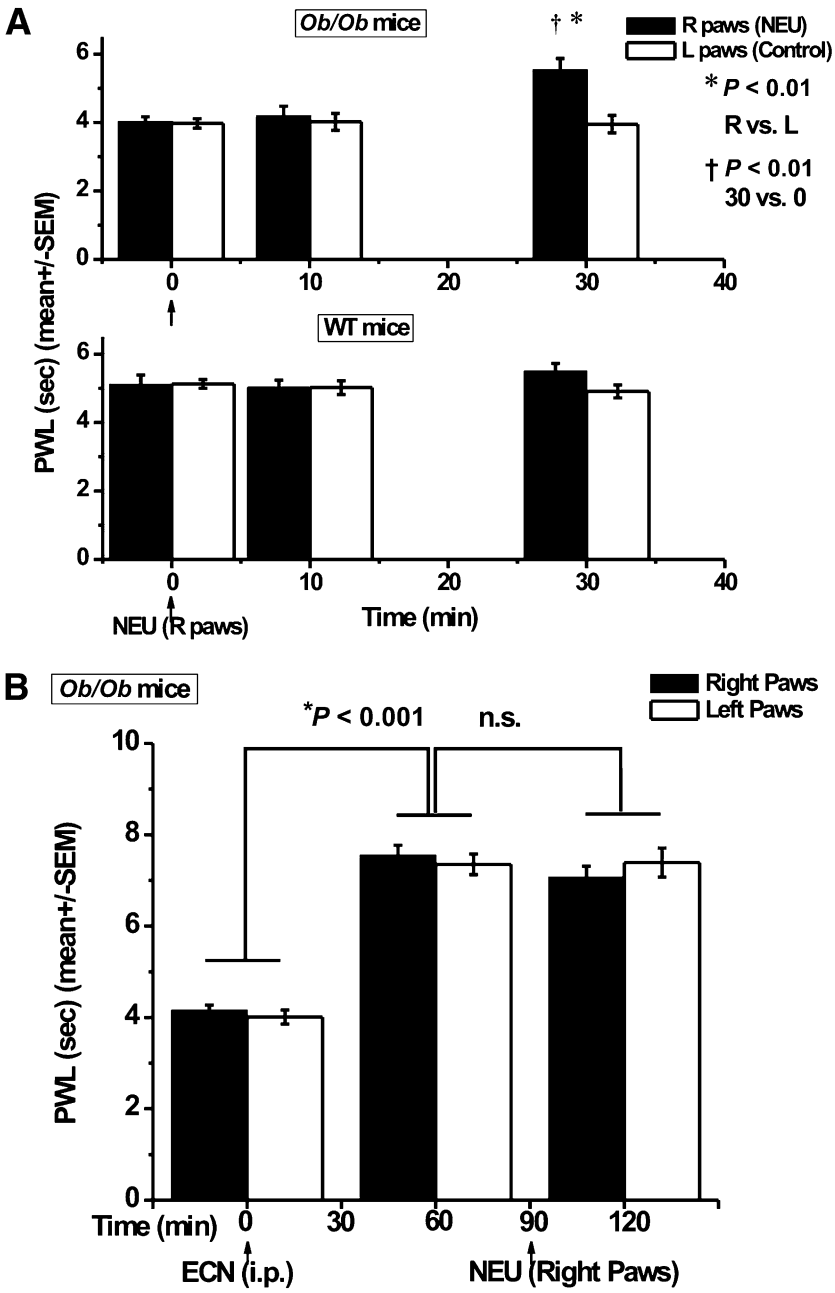

FIG. 8. NEU treatment in vivo reversed thermal hyperalgesia in diabetic *ob/ob* mice. *A*: The bar graphs with averaged data show that i.pl. injections of NEU completely reversed thermal hyperalgesia in diabetic *ob/ob* mice, while the same treatment was ineffective in WT mice. NEU was injected into right (R) paws, while uninjected left (L) paws served as controls. PWLs were determined in mice before (time point 0) and 10 and 30 min after injections of 10 μL NEU (arrows) into hind paws. Data are averages of seven experiments ±SEM. Symbols indicating significance of NEU treatments are as follows: *$P < 0.01$ for right vs. left paws at the same time points, and †$P < 0.01$ for data points at 30 min after NEU injections vs. 0 min. *B*: The bar graphs with averaged data show that injections of selective T-channel blocker ECN at 25 mg/kg i.p. completely reversed thermal hyperalgesia in diabetic *ob/ob* mice, as evidenced by elevated PWLs in both right and left paws ($P < 0.001$). Subsequent intraplantar injections of 1.5 units/mL NEU in the same animals did not significantly alter new baseline values of thermal PWLs (n.s., $P > 0.05$, $n = 4$). Arrows indicate times of injections of ECN and NEU.

multiple T-channel isoforms in spinal dorsal horn neurons may contribute to their hyperexcitability, which in turn may influence central sensitization of pain responses that is implicated in many pain disorders (27).

Overall, the results presented here fundamentally advance our understanding of the mechanisms of glycosylation underlying the posttranslational modification of $Ca_V3.2$ T-channels that has an important function in supporting peripheral nociceptive signaling. Our results strongly suggest that the manipulation of glycosylation states of peripheral nociceptors could be useful for the development of novel therapies for the treatment of painful PDN. This method may have an advantage over direct blockers of T-channels to suppress pain because NEU and related agents will correct the pathology of diabetes at its source rather than ameliorating the problem through separate pathways that also may be a source of unintended side effects. Our goal is to provide novel therapeutic modalities that would not only alleviate neuropathic pain in patients with diabetes but, even more importantly, also halt its progression without causing dangerous systemic side effects or creating the potential for drug abuse.

ACKNOWLEDGMENTS

This research is supported by American Diabetes Association 7-09-BS-190 (to S.M.T.), Dr. Harold Carron Endowment Fund, Priority Research Centers Program through the National Research Foundation of Korea (2012-0006690 to J.H.L.), National Institutes of Health grants 7-HL-036977 (to P.Q.B.) and GM-47969 (to D.F.C.), and funds from the Department of Anesthesiology at InJe University.

No potential conflicts of interest relevant to this article were reported.

P.O. researched data, wrote the manuscript, and contributed to discussion. H.P.O. researched data. W.E.M. researched data and contributed to and reviewed and edited the manuscript. M.O.J., R.S., M.M.J., W.J.C., J.L., S.-S.L., K.E.R., N.P., M.R.D., and K.K. researched data. D.F.C. researched data, contributed to discussion, and reviewed and edited the manuscript. J.-H.L. contributed to discussion and reviewed and edited the manuscript. P.Q.B. researched data, wrote the manuscript, and reviewed and edited the manuscript. V.J.-T. researched data, contributed to discussion, wrote the manuscript, and reviewed and edited the manuscript. S.M.T. researched data, wrote the manuscript, contributed to discussion, and reviewed and edited the manuscript. S.M.T. is the guarantor of this work and, as such, had full access to all the data in the study and takes responsibility for the integrity of the data and the accuracy of the data analysis.

Parts of this study were presented in abstract form at the 39th Annual Society for Neuroscience Meeting, Chicago, Illinois, 17–21 October 2009; the 40th Annual Society for Neuroscience Meeting, San Diego, California, 13–17 November 2010; the 2nd Conference on Calcium Channel Research, Placencia, Belize, 28 March–3 April 2010; and the 3rd Conference on Calcium Channel Research, Krabi, Thailand, 24–29 March 2013.

The authors thank Mr. Damir Bojadzic for technical assistance and Dr. Jan Redick and Dr. Stacey Guillot of the Advanced Microscopy Core Facility (University of Virginia) for help with imaging studies.

REFERENCES

1. Edwards JL, Vincent AM, Cheng HT, Feldman EL. Diabetic neuropathy: mechanisms to management. Pharmacol Ther 2008;120:1–34
2. Gooch C, Podwall D. The diabetic neuropathies. Neurologist 2004;10:311–322
3. Sima AA, Kamiya H. Diabetic neuropathy differs in type 1 and type 2 diabetes. Ann N Y Acad Sci 2006;1084:235–249
4. Todorovic SM, Jevtovic-Todorovic V. T-type voltage-gated calcium channels as targets for the development of novel pain therapies. Br J Pharmacol 2011;163:484–495
5. Latham JR, Pathirathna S, Jagodic MM, et al. Selective T-type calcium channel blockade alleviates hyperalgesia in ob/ob mice. Diabetes 2009;58:2656–2665
6. Nelson MT, Woo J, Kang H-W, et al. Reducing agents sensitize C-type nociceptors by relieving high-affinity zinc inhibition of T-type calcium channels. J Neurosci 2007;27:8250–8260
7. Todorovic SM, Lingle CJ. Pharmacological properties of T-type Ca^{2+} current in adult rat sensory neurons: effects of anticonvulsant and anesthetic agents. J Neurophysiol 1998;79:240–252
8. Robeva AS, Woodard R, Luthin DR, Taylor HE, Linden J. Double tagging recombinant A1- and A2A-adenosine receptors with hexahistidine and the FLAG epitope. Development of an efficient generic protein purification procedure. Biochem Pharmacol 1996;51:545–555
9. Moremen KW, Tiemeyer M, Nairn AV. Vertebrate protein glycosylation: diversity, synthesis and function. Nat Rev Mol Cell Biol 2012;13:448–462
10. Todorovic SM, Prakriya M, Nakashima YM, et al. Enantioselective blockade of T-type Ca^{2+} current in adult rat sensory neurons by a steroid that lacks γ-aminobutyric acid-modulatory activity. Mol Pharmacol 1998;54:918–927
11. Drel VR, Mashtalir N, Ilnytska O, et al. The leptin-deficient (ob/ob) mouse: a new animal model of peripheral neuropathy of type 2 diabetes and obesity. Diabetes 2006;55:3335–3343
12. Jacus MO, Uebele VN, Renger JJ, Todorovic SM. Presynaptic Cav3.2 channels regulate excitatory neurotransmission in nociceptive dorsal horn neurons. J Neurosci 2012;32:9374–9382
13. Jagodic MM, Pathirathna S, Nelson MT, et al. Cell-specific alterations of T-type calcium current in painful diabetic neuropathy enhance excitability of sensory neurons. J Neurosci 2007;27:3305–3316
14. Messinger RB, Naik AK, Jagodic MM, et al. In vivo silencing of the Ca(V)3.2 T-type calcium channels in sensory neurons alleviates hyperalgesia in rats with streptozocin-induced diabetic neuropathy. Pain 2009;145:184–195
15. Cao XH, Byun HS, Chen SR, Pan HL. Diabetic neuropathy enhances voltage-activated Ca2+ channel activity and its control by M4 muscarinic receptors in primary sensory neurons. J Neurochem 2011;119:594–603
16. Choe WJ, Messinger RB, Leach E, et al. TTA-P2 is a potent and selective blocker of T-type calcium channels in rat sensory neurons and a novel antinociceptive agent. Mol Pharmacol 2011;80:900–910
17. Hall KE, Sima AA, Wiley JW. Voltage-dependent calcium currents are enhanced in dorsal root ganglion neurones from the Bio Bred/Worchester diabetic rat. J Physiol 1995;486:313–322
18. Weis N, Black SA, Bladen C, Chen L, Zamponi GW. Surface expression and function of CaV3.2 T-type calcium channels are controlled by asparagine-linked glycosylation. Pflugers Arch-Euro J Physiol 2013;465:1159–70
19. Tyrrell L, Renganathan M, Dib-Hajj SD, Waxman SG. Glycosylation alters steady-state inactivation of sodium channel Nav1.9/NaN in dorsal root ganglion neurons and is developmentally regulated. J Neurosci 2001;21:9629–9637
20. Jing L, Chu XP, Jiang YQ, et al. N-glycosylation of acid-sensing ion channel 1a regulates its trafficking and acidosis-induced spine remodeling. J Neurosci 2012;32:4080–4091
21. Pertusa M, Madrid R, Morenilla-Palao C, Belmonte C, Viana F. N-glycosylation of TRPM8 ion channels modulates temperature sensitivity of cold thermoreceptor neurons. J Biol Chem 2012;287:18218–18229
22. Cohen DM. Regulation of TRP channels by N-linked glycosylation. Semin Cell Dev Biol 2006;17:630–637
23. Talley EM, Cribbs LL, Lee JH, Daud A, Perez-Reyes E, Bayliss DA. Differential distribution of three members of a gene family encoding low voltage-activated (T-type) calcium channels. J Neurosci 1999;19:1895–1911
24. Choi S, Na HS, Kim J, et al. Attenuated pain responses in mice lacking Ca(V)3.2 T-type channels. Genes Brain Behav 2007;6:425–431
25. Na HS, Choi S, Kim J, Park J, Shin HS. Attenuated neuropathic pain in Cav3.1 null mice. Mol Cells 2008;25:242–246
26. Wen XJ, Li ZJ, Chen ZX, et al. Intrathecal administration of Cav3.2 and Cav3.3 antisense oligonucleotide reverses tactile allodynia and thermal hyperalgesia in rats following chronic compression of dorsal root of ganglion. Acta Pharmacol Sin 2006; 27:1547–1552
27. Woolf CJ. Central sensitization: implications for the diagnosis and treatment of pain. Pain 2011;152(Suppl.):S2–S15